Electron-phonon thermalization in a scalable method for real-time quantum dynamics

Rizzi, V., Todorov, T. N., Kohanoff, J., & Correa, A. A. (2016). Electron-phonon thermalization in a scalable method for real-time quantum dynamics. *Physical Review B (Condensed Matter)*, *93*(2), [024306]. https://doi.org/10.1103/PhysRevB.93.024306

Published in:
Physical Review B (Condensed Matter)

Document Version:
Publisher's PDF, also known as Version of record

Queen's University Belfast - Research Portal:
Link to publication record in Queen's University Belfast Research Portal

Publisher rights
©2016 American Physical Society

General rights
Copyright for the publications made accessible via the Queen's University Belfast Research Portal is retained by the author(s) and / or other copyright owners and it is a condition of accessing these publications that users recognise and abide by the legal requirements associated with these rights.

Take down policy
The Research Portal is Queen's institutional repository that provides access to Queen's research output. Every effort has been made to ensure that content in the Research Portal does not infringe any person's rights, or applicable UK laws. If you discover content in the Research Portal that you believe breaches copyright or violates any law, please contact openaccess@qub.ac.uk.

Download date:04. May. 2023

Electron-phonon thermalization in a scalable method for real-time quantum dynamics

Valerio Rizzi,* Tchavdar N. Todorov, and Jorge J. Kohanoff
Atomistic Simulation Centre, Queen's University Belfast, Belfast BT7 1NN, Northern Ireland, United Kingdom

Alfredo A. Correa
Quantum Simulations Group, Lawrence Livermore National Laboratory, Livermore, California 94551, USA
(Received 25 June 2015; revised manuscript received 22 December 2015; published 27 January 2016)

We present a quantum simulation method that follows the dynamics of out-of-equilibrium many-body systems of electrons and oscillators in real time. Its cost is linear in the number of oscillators and it can probe time scales from attoseconds to hundreds of picoseconds. Contrary to Ehrenfest dynamics, it can thermalize starting from a variety of initial conditions, including electronic population inversion. While an electronic temperature can be defined in terms of a nonequilibrium entropy, a Fermi-Dirac distribution in general emerges only after thermalization. These results can be used to construct a kinetic model of electron-phonon equilibration based on the explicit quantum dynamics.

DOI: 10.1103/PhysRevB.93.024306

I. INTRODUCTION

Thermalization between electronic and vibrational degrees of freedom arises in a range of physical situations spanning widely different time and length scales. Examples include Joule heating and dissipation in solid-state and molecular physics [1,2], equilibration of warm dense matter generated by laser pulses [3–5], and radiation cascades [6]. The interest in coupled dynamics of out-of-equilibrium electrons with vibrations occurs in several fields, including transport in molecular junctions [7,8] and photoelectron spectroscopy [9], and has triggered the development of new experimental techniques [10]. Meanwhile, real-time atomistic simulations venture more and more often into nonequilibrium problems where accounting for electron-phonon thermalization is crucial [11]. A choice of methods can capture the interaction between electrons and vibrations, from the phenomenological Boltzmann equation in extended systems [12] to its counterpart at the nanoscale, i.e., nonequilibrium Green's functions (NEGFs) [13].

Nevertheless, the problem of thermal equilibration between interacting degrees of freedom (DOF) is particularly difficult to tackle from the simulation point of view. For purely classical systems simulated via molecular dynamics, anharmonicities in the potential lead—not without technical problems—to thermalization and energy equipartition [14]. In harmonic or weakly anharmonic systems, equilibration does not happen spontaneously: it requires the introduction of external thermostats. The situation is even more complicated for quantum interacting systems and it becomes especially critical in mixed quantum-classical approaches. A widely used approach is the macroscopic two-temperature model where nuclear and electronic motion is represented in terms of temperature fields coupled via appropriate diffusion equations [15,16]. This together with the introduction of Langevin thermostats [17] has proved successful in interpreting measured quantities [18,19]. This approach remains of active interest and, in recent years, it has evolved into more elaborate methodologies where the nuclear motion is taken into account via classical molecular dynamics simulations, while electrons are treated at increasing levels of sophistication [20–25].

The simplest approach to nonadiabatic electron-nuclear atomistic simulation is Ehrenfest dynamics (ED) [1] in which classical nuclei interact with the mean electron density. ED is tractable and simple but it fails to describe the spontaneous decay of electronic excitations into phonons because of the lack of microscopic detail in the electronic density and resultant loss of electron-nuclear correlation [26]. Vibrational DOF spontaneously cool down at the expense of increasing the electronic energy, violating the second law of thermodynamics. Missing in ED are the collisions that drive the probability distribution function towards equilibrium. The approach to equilibrium can be reinstated via Boltzmann's kinetic theory, i.e., through phenomenological relaxation dynamics. However, to recover this in microscopic dynamics for a closed system requires thermostating techniques; for quantum DOF, this introduces an additional layer of complexity.

Correlated electron-ion dynamics (CEID) [26,27] is a method that was developed to go beyond ED. It starts from the bare electron-nuclear Hamiltonian and solves it approximately by a perturbative expansion in powers of nuclear fluctuations about the mean trajectory. However, it scales between quadratically and cubically with the number of nuclear DOF, becoming prohibitive beyond a few DOF, along with difficulties in the choice of closure strategy for the hierarchy of perturbative equations of motion. The computational bottleneck persists in alternative expansion strategies for the electron-nuclear problem [28].

Today there is a new impetus in the study of mesoscale systems, as their technological applications and simulation capability meet [29]. These systems mark a difficult middle ground between bulk and the atomic scale. There is a serious need for a methodology that includes the mechanisms of thermal equilibration between electron and phonon DOF, and at the same time is amenable to computer simulation with present-day resources [30]. This need for an efficient approach to the dynamics of thermalization at the mesoscale

*Corresponding author: vrizzi01@qub.ac.uk

 ©2016 American Physical Society

has motivated us to develop a microscopic method for coupled real-time quantum electron-phonon dynamics. We refer to it as effective CEID (ECEID).

ECEID advances beyond CEID in terms of conceptual and computational tractability by exploiting a different starting point: a system of electrons and harmonic vibrations, coupled by an interaction that is linear in the generalized displacements. This more specialized scenario maintains applicability to the large family of problems involving harmonic nuclear motion, while offering important advantages. This Hamiltonian starts from the Born-Oppenheimer level of description, with the role of the coupling being to generate the nonadiabatic corrections. By contrast, the old CEID method above had the dual challenge of first generating the Born-Oppenheimer behavior (starting from the bare full Hamiltonian) and then also going beyond. Furthermore, ECEID employs a nonperturbative closure strategy, which enables the coupled electron-phonon dynamics to be formulated in terms of a set of variables and equations of motion that scale linearly with the number of vibrational DOF. This opens the possibility of tackling problems previously out of reach: in test runs, we have been able to simulate up to 600 electrons interacting with 100 vibrational DOF on the picosecond time scale, on an ordinary workstation. The next section introduces the method, followed by examples, and critical comparisons with ED and with a kinetic model in Sec. III. Section IV gives a summary and concluding remarks.

II. THE ECEID METHOD

To describe the ECEID method in its most general form, we start from the Hamiltonian

$$\hat{H} = \underbrace{\hat{H}_{\rm e} + \sum_{\nu=1}^{N_{\rm o}} \left(\frac{\hat{P}_\nu^2}{2M_\nu} + \frac{1}{2} K_\nu \hat{X}_\nu^2 \right)}_{\hat{H}_0} - \sum_{\nu=1}^{N_{\rm o}} \hat{F}_\nu \hat{X}_\nu. \tag{1}$$

Here, $\hat{H}_{\rm e}$ is a general interacting or noninteracting many-electron Hamiltonian in the absence of vibrations. $\hat{X}_\nu$ and $\hat{P}_\nu$ are displacement and canonical momentum operators for oscillator ν, with mass M_ν and spring constant K_ν, coupled linearly to the electrons via the electronic operator $\hat{F}_\nu$. $N_{\rm o}$ is the number of blue harmonic vibrational DOF. Any harmonic Hamiltonian in the vibrational DOF can be brought into this form through a change of generalized coordinates.

The electronic density matrix (DM) $\hat{\rho}_{\rm e}(t) = {\rm Tr}_{\rm o}(\hat{\rho}(t))$ is obtained from the full electron-phonon DM $\hat{\rho}(t)$ by tracing over the oscillator degrees of freedom and obeys the effective Liouville equation [26]

$$\dot{\hat{\rho}}_{\rm e}(t) = \frac{1}{i\hbar} [\hat{H}_{\rm e}, \hat{\rho}_{\rm e}(t)] - \frac{1}{i\hbar} \sum_{\nu=1}^{N_{\rm o}} [\hat{F}_\nu, \hat{\mu}_\nu(t)], \tag{2}$$

where $\hat{\mu}_\nu(t) = {\rm Tr}_{\rm o}[\hat{X}_\nu \hat{\rho}(t)]$. The full DM can be written exactly as

$$\hat{\rho}(t) = e^{-\frac{i}{\hbar}\hat{H}_0 t} \hat{\rho}(0) e^{\frac{i}{\hbar}\hat{H}_0 t} - \frac{1}{i\hbar} \sum_{\nu=1}^{N_{\rm o}} \int_0^t e^{\frac{i}{\hbar}\hat{H}_0(\tau - t)} \times [\hat{F}_\nu \hat{X}_\nu, \hat{\rho}(\tau)]\, e^{-\frac{i}{\hbar}\hat{H}_0(\tau - t)} d\tau. \tag{3}$$

We require equations of motion (EOM) for $\hat{\rho}_{\rm e}(t)$ and the mean oscillator occupations $N_\nu(t) = {\rm Tr}(\hat{N}_\nu \hat{\rho}(t))$, where $\hat{N}_\nu = \hat{a}_\nu^\dagger \hat{a}_\nu$ with $\hat{a}_\nu^\dagger$ ($\hat{a}_\nu$) the creation (annihilation) operator for oscillator ν. To close the equations, we place (3) in the definition of $\hat{\mu}_\nu(t)$ above and make three approximations. First, in $\hat{\mu}_\nu(t)$—but not earlier—we put $\hat{\rho}(\tau) \approx \hat{\rho}_{\rm e}(\tau)\hat{\rho}_{\rm o}(\tau)$. This retains electron-phonon correlation exactly to lowest order in the coupling $\hat{F}_\nu$, and approximately to higher order, in analogy with the self-consistent Born approximation [1]. Second, after taking oscillator traces, we retain only terms diagonal in ν, suppressing electron-mediated phonon-phonon correlation. Third, we neglect terms of the form $\langle \hat{a}_\nu \hat{a}_\nu \rangle$, $\langle \hat{a}_\nu^\dagger \hat{a}_\nu^\dagger \rangle$, retaining only single-phonon processes and excluding anharmonicity. From this point, ν is omitted for simplicity of notation.

These approximations correspond to the low electron-phonon coupling limit and yield

$$\hat{\mu}(t) = \frac{i}{M\omega} \int_0^t \left(N(\tau) + \frac{1}{2} \right) e^{\frac{i}{\hbar}\hat{H}_{\rm e}(\tau - t)} \times [\hat{F}, \hat{\rho}_{\rm e}(\tau)] e^{-\frac{i}{\hbar}\hat{H}_{\rm e}(\tau - t)} \cos\omega(\tau - t) d\tau - \frac{1}{2M\omega} \int_0^t e^{\frac{i}{\hbar}\hat{H}_{\rm e}(\tau - t)} \times \{\hat{F}, \hat{\rho}_{\rm e}(\tau)\} e^{-\frac{i}{\hbar}\hat{H}_{\rm e}(\tau - t)} \sin\omega(\tau - t) d\tau, \tag{4}$$

where $\omega = \sqrt{K/M}$ is the oscillator angular frequency. The full derivation of Eq. (4) is given in Appendix A.

We calculate $\hat{\mu}(t)$ as follows. We introduce four auxiliary electronic operators $(\hat{C}_{\rm c}, \hat{A}_{\rm c}, \hat{C}_{\rm s}, \hat{A}_{\rm s})$ per oscillator, defined by

$$\hat{C}_{\rm c}(t) = \int_0^t \left(N(\tau) + \frac{1}{2} \right) e^{\frac{i}{\hbar}\hat{H}_{\rm e}(\tau - t)} \times [\hat{F}, \hat{\rho}_{\rm e}(\tau)] e^{-\frac{i}{\hbar}\hat{H}_{\rm e}(\tau - t)} \cos\omega(\tau - t) d\tau, \tag{5}$$

$$\hat{A}_{\rm c}(t) = \frac{1}{2} \int_0^t e^{\frac{i}{\hbar}\hat{H}_{\rm e}(\tau - t)} \{\hat{F}, \hat{\rho}_{\rm e}(\tau)\} e^{-\frac{i}{\hbar}\hat{H}_{\rm e}(\tau - t)} \cos\omega(\tau - t) d\tau, \tag{6}$$

with $\hat{C}_{\rm s}$ and $\hat{A}_{\rm s}$ obtained by replacing cosine with sine above. They obey the EOM

$$\dot{\hat{C}}_{\rm c}(t) = -\frac{i}{\hbar} [\hat{H}_{\rm e}, \hat{C}_{\rm c}(t)] + \omega \hat{C}_{\rm s}(t) + \left(N(t) + \frac{1}{2} \right) [\hat{F}, \hat{\rho}_{\rm e}(t)], \tag{7}$$

$$\dot{\hat{C}}_{\rm s}(t) = -\frac{i}{\hbar} [\hat{H}_{\rm e}, \hat{C}_{\rm s}(t)] - \omega \hat{C}_{\rm c}(t), \tag{8}$$

$$\dot{\hat{A}}_{\rm c}(t) = -\frac{i}{\hbar} [\hat{H}_{\rm e}, \hat{A}_{\rm c}(t)] + \omega \hat{A}_{\rm s}(t) + \frac{1}{2} \{\hat{F}, \hat{\rho}_{\rm e}(t)\}, \tag{9}$$

$$\dot{\hat{A}}_{\rm s}(t) = -\frac{i}{\hbar} [\hat{H}_{\rm e}, \hat{A}_{\rm s}(t)] - \omega \hat{A}_{\rm c}(t), \tag{10}$$

and, in terms of these quantities, (4) becomes

$$\hat{\mu}(t) = \frac{1}{M\omega} (i\, \hat{C}_{\rm c}(t) - \hat{A}_{\rm s}(t)). \tag{11}$$

Analogous steps lead to

$$\dot{N}(t) = \frac{1}{M\hbar\omega} \left(i\, {\rm Tr}_{\rm e}(\hat{F}\hat{C}_{\rm s}(t)) + {\rm Tr}_{\rm e}(\hat{F}\hat{A}_{\rm c}(t)) \right), \tag{12}$$

giving an EOM for the oscillator occupation numbers. This closes the system of EOM. Energy conservation is discussed in Appendix B.

A. Comparison with Ehrenfest dynamics

The terms involving $[\hat{F},\hat{\rho}_e(t)]$ are related to the electronic friction (an effective dissipative force due to electron-hole excitations by the oscillator), while those with $\{\hat{F},\hat{\rho}_e(t)\}$ cause electronic noise and spontaneous phonon emission [31,32].

To see this, consider the above problem within Ehrenfest dynamics: electrons interacting with a classical oscillator, with phase ϕ, slowly varying amplitude A, displacement $X(t) = A\sin(\omega t-\phi)$, and velocity $V(t)=\dot{X}(t)$. Next, average over ϕ to sample different initial conditions. The counterpart of the earlier approximations reads $\langle X(t)X(\tau)\hat{\rho}_e(\tau,\phi)\rangle_\phi \approx \langle X(t)X(\tau)\rangle_\phi\hat{\rho}_e(\tau)$, together with suppression of oscillator position-momentum correlations. This produces (11) *without* the second term, and with N given by $(N+1/2)\hbar\omega = M\omega^2A^2/2$. The phase-averaged power into the Ehrenfest oscillator, $\langle V(t)F(t)\rangle_\phi$ with $F(t)=\mathrm{Tr}_e(\hat{F}\hat{\rho}_e(t,\phi))$, becomes (12) without the second term. Finally, the remaining first term in (12) is the same as the mean rate of work by the electronic friction force due to the symmetric part of the velocity-dependent force kernel in Eq. (16) in [32]. Thus the ECEID EOM, with the anticommutator in (9) suppressed, describe ED (with the oscillator phase averaged out), physically dominated by electron-hole excitations and electronic friction.

The second term in (12) corresponds instead to the power delivered to the oscillators by the effective electronic-noise force described by line 1 of Eq. (56) in [32]: the key correction beyond the mean-field ED. The competition between the two terms in (12) enables thermodynamic electron-phonon equilibration [32], which is thus built into the ECEID method.

B. From many-electron to one-electron equations of motion

The EOM above are still many-electron equations. To be able to apply the method to systems with large numbers of electrons, as a practical necessity we express the EOM in one-electron form. We do this by tracing out all but one electron through $N_e\mathrm{Tr}_{e,2,\ldots,N_e}$, where N_e is the number of electrons. If $\hat{H}_e$ and $\hat{F}$ are one-body operators, all operators in the EOM can now be replaced by their one-electron counterparts, except for the anticommutator term in Eq. (9), $\{\hat{F},\hat{\rho}_e\}$. Following [26], it transforms into

$$\left\{\hat{F}^{(1)}(1),\hat{\rho}_e^{(1)}(1)\right\} + 2\mathrm{Tr}_{e,2}\left(\hat{F}^{(1)}(2)\hat{\rho}_e^{(2)}(1,2)\right), \qquad (13)$$

where superscripts $^{(1)}$ and $^{(2)}$ denote, respectively, one- and two-electron operators. The simplest decoupling for the two-particle DM is

$$\hat{\rho}_e^{(2)}(12,1'2') = \hat{\rho}_e^{(1)}(11')\hat{\rho}_e^{(1)}(22') - \hat{\rho}_e^{(1)}(12')\hat{\rho}_e^{(1)}(21'), \qquad (14)$$

which is valid for independent electrons. Using this in (13), we obtain $\{\hat{F},\hat{\rho}_e(t)\} - 2\hat{\rho}_e(t)\hat{F}\hat{\rho}_e(t)$, where now $\hat{\rho}_e(t)$ is the one-electron DM and all other operators are also one-electron operators.[1] The accuracy of (14) reduces with increased electron-phonon coupling; corrections are discussed in [27].

Screening can be included in a one-electron mean-field picture within a Hartree-Fock scheme following [27], or in a time-dependent density functional framework [33].

To simulate a finite system, we must account for the level broadening and decoherence introduced by the environment. We replace $[\hat{H}_e,\hat{Q}]$ in (7)–(10) by $\hat{H}_\Gamma\hat{Q}-\hat{Q}\hat{H}_\Gamma^\dagger$, where $\hat{Q} = (\hat{C}_c,\hat{A}_c,\hat{C}_s,\hat{A}_s)$, $\hat{H}_\Gamma = \hat{H}_e - i\Gamma\hat{I}_{\mathrm{leads}}$, and $\hat{I}_{\mathrm{leads}}$ is the identity operator in the leads with Γ a small positive quantity. The total energy $E = E_e + E_o + E_c$, where $E_e = \mathrm{Tr}_e(\hat{H}_e\hat{\rho}_e(t))$, $E_o = \sum_\nu \hbar\omega_\nu(N_\nu(t)+1/2)$, and $E_c = -\sum_\nu \mathrm{Tr}_e(\hat{F}_\nu\hat{\mu}_\nu(t))$, is identically conserved, provided the damping self-energy and the electron-phonon coupling $\hat{F}$ lie in different subspaces. The derivation of this result is shown in Appendix B. In our examples, once Γ exceeds the energy-level spacing in the system, transition rates resulting from ECEID dynamics become independent of Γ. The role of Γ is to mimic an extended (infinitely large) system without the extra cost.

III. RESULTS

Here we have implemented the ECEID method for the discretized electron-phonon Hamiltonian (15),

$$\hat{H}_{e\text{-}ph} = \overbrace{\sum_{ij}\alpha_{ij}\hat{c}_i^\dagger\hat{c}_j}^{\hat{H}_e} - \sum_{\nu ij}\overbrace{F_{\nu ij}\hat{c}_i^\dagger\hat{c}_j\,\frac{\hat{a}_\nu^\dagger+\hat{a}_\nu}{\sqrt{2M_\nu\omega_\nu/\hbar}}}^{\hat{F}_\nu\hat{X}_\nu} + \sum_\nu \hbar\omega_\nu\left(\hat{a}_\nu^\dagger\hat{a}_\nu+\frac{1}{2}\right), \qquad (15)$$

where $\hat{c}^\dagger(\hat{c})$ are the fermion creation (annihilation) operators. α_{ij} are on-site energies and hoppings with $\{i,j\}$ running over the atomic sites. The electronic DM evolves according to Eq. (2). $\hat{\mu}_\nu(t)$ is calculated using Eq. (11), which is obtained from the time evolution of the auxiliary operators (7)–(10). These enter also in the EOM for the mean oscillator occupation (12). The number of EOM scales linearly with N_o and so does the computational cost.

We use these equations to simulate nonequilibrium electron-phonon dynamics in the model in Fig. 1: a wire with an electronic half-filled band with 96 spin-degenerate noninteracting electrons coupled to 15 harmonic oscillators. The integration of the EOM is highly efficient and parallelizable over the different oscillators. On a modern 20 processor machine, a 10 ps simulation requires about one hour.

To track the evolution of the two subsystems, we use two temperaturelike parameters: T_o^{quant} for the oscillators and T_e for electrons. If $\overline{N}(t) = \sum_{\nu=1}^{N_o} N_\nu(t)/N_o$, then the oscillator

[1] Here we ignore the additional term $\hat{\rho}_e(t)\,\mathrm{Tr}_e(\hat{F}\hat{\rho}_e(t))$. It corresponds to the so-called Hartree diagram in NEGF treatments of electron-phonon interactions [13], and is related to motion of the oscillator centroid, a mean-field property. This term involves the mean force $\mathrm{Tr}_e(\hat{F}\hat{\rho}_e(t))$ on a given degree of freedom, which in the present examples is orders of magnitude less than a typical interatomic bond force.

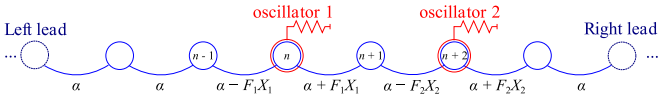

FIG. 1. Schematic of our model system: a nearest-neighbor one-dimensional lattice model of an atomic wire divided into a central region between two leads. This embeds the sample in an environment and provides the framework for future transport calculations. Each of the three regions has 32 sites, with 15 equispaced harmonic oscillators coupled to the central region. Oscillator ν couples to site n_ν through $\hat{F}_\nu = F_\nu(\hat{c}^\dagger_{n_\nu+1}\hat{c}_{n_\nu} + \hat{c}^\dagger_{n_\nu}\hat{c}_{n_\nu+1} - \hat{c}^\dagger_{n_\nu}\hat{c}_{n_\nu-1} - \hat{c}^\dagger_{n_\nu-1}\hat{c}_{n_\nu})$, which corresponds to independent atomic motion in a lattice description. The extension from Einstein oscillators to normal modes is straightforward. The on-site energies are uniform; the hoppings $\alpha = -1$ eV and $\Gamma = 0.08$ eV. For all of the oscillators, $M = 0.5$ a.m.u., $\hbar\omega = 0.2$ eV, and $F = 0.3$ eV/Å.

temperature is defined through $\overline{N}(t) = (e^{\hbar\omega/k_B T_o^{\rm quant}(t)} - 1)^{-1}$. In the Ehrenfest case, this definition breaks down when the energy of the classical oscillators goes down to 0 and $\overline{N}(t) \to -1/2$. For that case, we employed an alternative semiclassical definition of oscillator temperature, $k_B T_o^{\rm class} = (\overline{N}(t) + \frac{1}{2})\hbar\omega$. The electronic temperature is taken from $T_e = \Delta E_e/\Delta S_e$, where ΔE_e is the variation over five time steps in electronic energy and ΔS_e is the corresponding variation in electronic von Neumann entropy, $S_e = -k_B \sum_n [f_n \ln f_n + (1 - f_n)\ln(1 - f_n)]$, where f_n are the diagonal elements of $\hat{\rho}_e$ in the basis of $\hat{H}_e$ eigenstates, the occupations of the unperturbed electronic energy levels. T_e is then inferred from a running average of its reciprocal. We note that these temperatures are only observables, not an input into the simulation.

As the system evolves, no macroscopic work is done, but energy (heat) is exchanged between the electronic and the oscillators subsystems. Having a microscopic definition of the entropy also allows us to give a time-local quantification of the rate of heat exchange, $J_Q = \frac{dS_{\rm total}}{dt}/(1/T_o - 1/T_e)$, where $dS_{\rm total} = dS_o + dS_e$. In the weak-coupling limit, where the correlation energy E_c is small, the heat current reduces to $J_Q = dE_o/dt$, and, on average, $dE_o/dt = -dE_e/dt$.

A. Thermalization

Our first example starts with $T_e = 10\,000$ K and $T_o^{\rm class} = 1400$ K. This mimics a common situation in laser or irradiation experiments in which electrons initially absorb energy faster that ions. In Fig. 2, we compare the time evolution of the temperature for ED and ECEID. After a short transient which depends on the details of the initial state, a long-lived steady state develops with a net energy flow from one subsystem to the other. In ED, the absence of electronic noise [second term in Eq. (12)] results in a heat flow going in the wrong direction: from the cold oscillators into the hot electrons, until the oscillators reach green temperature. In ECEID, the inclusion of the electronic noise makes the exchange of heat physical and the final thermalization possible [Fig. 2(a)]. The heat flow scales linearly with the temperature difference (Fourier's law) [Fig. 2(c)]. In the equilibrium state reached in ECEID, the two final temperatures agree within 1%.

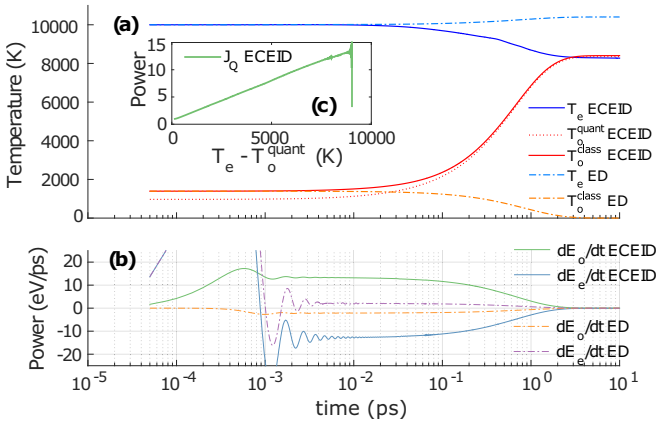

FIG. 2. Coupled dynamics of a closed system of electrons and oscillators with the parameters given in the text. (a) Time evolution of the electronic and oscillators temperature for ECEID and the phase-averaged ED discussed above. (b) Rate of change of electronic and oscillators energies. After a transient of 10 fs, the systems evolve until eventually an equilibrium state (ECEID) or an unphysical state (ED) is reached. (c) For ECEID, a clear linear scaling (Fourier law behavior) is observed for heat flow vs temperature difference (up to a time of 2.5 ps). The noise for high-temperature differences is related to the initial transient.

B. Population inversion

Next, we test an extremely out-of-equilibrium phenomenon: a complete population inversion. Initially, the electrons occupy the upper half of the energy states in the wire, corresponding to an infinitesimal negative electronic temperature. The oscillators are held at $N = 0.5$, or $T_o^{\rm quant} = 2112$ K, throughout. This simulates coupling to an infinitely efficient external thermostat, thus isolating just the electron dynamics. Figure 3 shows snapshots of the electronic population dynamics and the temperature. The electrons deexcite in both ECEID and ED. In ED, this happens through negative friction [34]. Comparing Figs. 3(a) and 3(b) at 0.5 ps, we see that the deexcitation is faster in ECEID; this is because ECEID also includes the contribution from spontaneous phonon emission. But the crucial difference is the final state: ECEID correctly takes the electrons all the way down to a Fermi-Dirac distribution corresponding to the oscillator temperature; ED by contrast gets stuck at a distribution with roughly uniform occupancies [35]. These two ED features have a common origin. If electronic occupancies $f(E)$ depend only on energy E, then a rearrangement of the result for the electronic friction in [8] gives an integral containing $f'(E)$ as a factor in the integrand; hence the opposite signs for the friction, at small negative and small positive temperatures, and hence also the unphysical "equilibration" of the electrons at $f'(E) = 0$ in ED, when the friction vanishes and the main electron-phonon interaction mechanism present in ED goes to zero.

The role of Γ in these simulations is crucial for thermalization because it provides a controlled way to embed a finite system that would not equilibrate into an extended one that does. In Fig. 4, we study the time evolution of a sample of electronic states in ECEID for $\Gamma = 0.08$ and $\Gamma = 0.8$ eV for the same initial population inversion as above. The results are

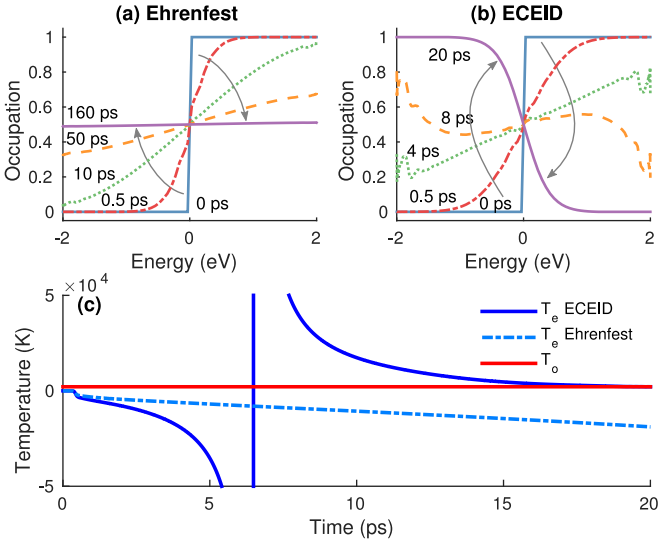

FIG. 3. Population inversion simulation with the oscillators held at constant temperature. We show snapshots of the population of the electronic states in (a) ED at 0, 0.5, 10, 50, and 160 ps, and (b) ECEID at 0, 0.5, 4, 8, and 20 ps. (The arrows highlight the overall initial-to-final transition in each case.) (c) Temperature evolution during the simulation for ED and ECEID compared with the fixed oscillator temperature.

almost superimposable: for Γ larger than the average level spacing $\sim$0.04 eV, ECEID is largely independent of Γ. We observed that the dynamics of any level j is exactly symmetric with that of level $96-j+1$ for all times.

C. Kinetic model

The rich pattern of population evolutions shown in Fig. 4 can be compared with a kinetic model of the transitions between electronic levels due to phonon absorption and emission. The rate equation for the population f_j of level j is

$$\dot{f}_j(t) = \sum_k \frac{1}{\tau_{jk}}[-Nf_j(1-f_k) + (N+1)f_k(1-f_j)] + \frac{1}{\tau_{kj}}[Nf_k(1-f_j) - (N+1)f_j(1-f_k)]. \quad (16)$$

The scattering rates $1/\tau_{jk} = (\pi/M\omega)N_o|F_{jk}|^2 G_{jk}$ are given by the Fermi golden rule (FGR). $|F_{jk}|^2$ can be calculated analytically by using plane-wave states with energies $E_j = 2\alpha\cos\phi_j$, (dimensionless) crystal momentum $\phi_j = j\pi/97$, $j = 1,\ldots,96$, and by averaging over the two opposite signs of momentum for the final state. $G_{jk} = e^{-[(E_k-E_j-\hbar\omega)/\Delta]^2}/(\sqrt{\pi}\Delta)$ is a Gaussian envelope with a width Δ. It mimics the δ function that appears in the FGR electron-phonon transition rates. We plug the parameters of the population inversion simulation from Fig. 3 into the kinetic model with $\Delta = 0.08$ eV and in Fig. 4 we compare it with ECEID simulations, showing close agreement.

The comparison with the kinetic model illustrates that ECEID, owing to its scalability, can access time and size domains where macroscopic thermodynamic behavior is beginning to emerge. In addition, the direct comparison between inherently different descriptions provides a bottom-up path to a validation, at the atomistic level, of kinetic models of electron-phonon dynamics, without having to resort to the relaxation-time approximation.

The response is fastest for states in the middle of the band, where the step in the initial population is. The time that these states take to settle into a long-lived half-occupied steady state—about 0.5 ps—is comparable to the time needed for the initial temperature response, i.e., the small initial steplike feature in the blue results in Fig. 3(c). (This transient response in the electron-phonon dynamical simulation is absent in FGR because FGR by construction describes mean transition rates in the long-time limit.) The results of the kinetic model show little variation over the range $0.04 < \Delta < 0.15$ eV or for different shapes of G_{jk}. For this choice of parameters, the kinetic model captures the main physics of the problem. The combination of the kinetic model and ECEID provides a direct way to construct rate equations that allow thermodynamic electron-phonon equilibration on the basis of a real-time quantum mechanical simulation.

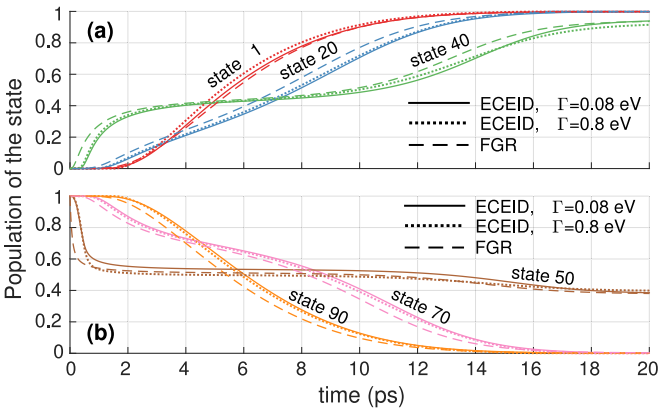

FIG. 4. Comparison of the dynamics of electronic states for ECEID with $\Gamma = 0.08$ eV, ECEID with $\Gamma = 0.8$ eV, and the kinetic model starting from an inverted population. In (a), we track state 1, state 20, and state 40; in (b), we track state 90, state 70, and state 50.

IV. CONCLUSION

Our method can track the dynamics of interacting out-of-equilibrium quantum many-body systems of electrons and oscillators in real time. We have applied it to nanowires from a range of initial conditions to demonstrate its ability to describe thermalization. We show how an entropic definition of temperature, combined with the microscopic ECEID dynamics, produces a thermodynamically meaningful description of the energy exchange between the two subsystems, and their equilibration. A key aspect of the method is the linear scaling with the number of vibrational DOF. This makes it possible to access large size and time domains where macroscopic transition dynamics is beginning to emerge and where ECEID provides a basis for suitable kinetic models. In contrast with kinetic models, ECEID also applies to problems

dominated by quantum coherence, such as electron transport in atomic-scale open systems. An implementation of ECEID for current-carrying systems is under development.

ACKNOWLEDGMENTS

We thank Lorenzo Stella and Kieron Burke for helpful discussions. We express our gratitude to the Leverhulme Trust for funding this research under Grant No. RPG-2012-583. Work by V.R. (during a visit hosted by A.A.C.) and by A.A.C. is performed under the auspices of the U.S. Department of Energy by Lawrence Livermore National Laboratory under Contract No. DE-AC52-07NA27344.

APPENDIX A: DERIVATION OF $\hat{\boldsymbol{\mu}}(t)$

For convenience, below we use the notation

$$\hat{Q}^t = e^{\frac{i}{\hbar}\hat{H}_0 t}\hat{Q}e^{-\frac{i}{\hbar}\hat{H}_0 t} \tag{A1}$$

for a generic operator $\hat{Q}$. Inserting Eq. (3) into the definition of $\hat{\mu}_\nu(t)$, we get

$$\hat{\mu}_\nu(t) = -\frac{1}{i\hbar}\,\mathrm{Tr_o}\left(\hat{X}_\nu \sum_{\nu'=1}^{N_o}\int_0^t \left[\hat{F}_{\nu'}^{\tau-t}\hat{X}_{\nu'}^{\tau-t},\hat{\rho}^{\tau-t}(\tau)\right]d\tau\right). \tag{A2}$$

Here we assume, for simplicity, that the unperturbed motion described by $\hat{\rho}^{-t}(0)$ in (3) does not contribute to motion of the oscillator centroids and to $\hat{\mu}(t)$.

We expand the commutator and permute the operators within the oscillator trace in Eq. (A2) to obtain

$$\hat{\mu}_\nu(t) = -\frac{1}{i\hbar}\,\mathrm{Tr_o}\sum_{\nu'=1}^{N_o}\left(\int_0^t \hat{F}_{\nu'}^{\tau-t}\hat{X}_\nu\hat{X}_{\nu'}^{\tau-t}\hat{\rho}^{\tau-t}(\tau)d\tau - \int_0^t \hat{\rho}^{\tau-t}(\tau)\hat{X}_{\nu'}^{\tau-t}\hat{X}_\nu\hat{F}_{\nu'}^{\tau-t}d\tau\right). \tag{A3}$$

By time-differentiating $\hat{X}_{\nu'}^{\tau-t}$ twice and using the canonical position-momentum commutation relation $[\hat{X}_\nu,\hat{P}_{\nu'}] = i\hbar\delta_{\nu\nu'}$, we can see that

$$\ddot{\hat{X}}_\nu^{\tau-t} = -\frac{K_\nu}{M_\nu}\hat{X}_\nu^{\tau-t}. \tag{A4}$$

The solution of (A4), with the initial conditions $\hat{X}_\nu^0 = \hat{X}_\nu$ and $\dot{\hat{X}}_\nu^0 = \hat{P}_\nu/M_\nu$ and with the introduction of the characteristic oscillator frequency $\omega_\nu = \sqrt{K_\nu/M_\nu}$, is

$$\hat{X}_\nu^{\tau-t} = \hat{X}_\nu\cos\omega_\nu(\tau-t) + \frac{\hat{P}_\nu}{M_\nu\omega_\nu}\sin\omega_\nu(\tau-t), \tag{A5}$$

which can be rewritten in second quantization as

$$\hat{X}_\nu^{\tau-t} = \sqrt{\frac{\hbar}{2M_\nu\omega_\nu}}(\hat{a}_\nu^\dagger e^{i\omega_\nu(\tau-t)} + \hat{a}_\nu e^{-i\omega_\nu(\tau-t)}). \tag{A6}$$

Now we apply the decomposition

$$\hat{A}\hat{B} = \tfrac{1}{2}\{\hat{A},\hat{B}\} + \tfrac{1}{2}[\hat{A},\hat{B}] \tag{A7}$$

to both $\hat{X}_\nu\hat{X}_{\nu'}^{\tau-t}$ and $\hat{X}_{\nu'}^{\tau-t}\hat{X}_\nu$ in Eq. (A3), leading to

$$\hat{\mu}_\nu(t) = -\frac{1}{2i\hbar}\,\mathrm{Tr_o}\sum_{\nu'=1}^{N_o}\left(\int_0^t \left[\hat{F}_{\nu'}^{\tau-t},\hat{\rho}^{\tau-t}(\tau)\right]\left\{\hat{X}_\nu,\hat{X}_{\nu'}^{\tau-t}\right\}d\tau\right) - \frac{1}{2M_\nu\omega_\nu}\mathrm{Tr_o}\left(\int_0^t \left\{\hat{F}_\nu^{\tau-t},\hat{\rho}^{\tau-t}(\tau)\right\}\sin\omega_\nu(\tau-t)d\tau\right), \tag{A8}$$

where we have used

$$\sum_{\nu'=1}^{N_o}\left[\hat{X}_\nu,\hat{X}_{\nu'}^{\tau-t}\right] = \frac{i\hbar}{M_\nu\omega_\nu}\sin\omega_\nu(\tau-t). \tag{A9}$$

Equation (A8) is exact.

The approximation $\hat{\rho}(\tau)\approx\hat{\rho}_e(\tau)\hat{\rho}_o(\tau)$ given in the main text is now made in Eq. (A8), yielding

$$\hat{\mu}_\nu(t) = -\frac{1}{2i\hbar}\sum_{\nu'=1}^{N_o}\int_0^t \left[\hat{F}_{\nu'}^{\tau-t},\hat{\rho}_e^{\tau-t}(\tau)\right]\mathrm{Tr_o}\left(\hat{\rho}_o^{\tau-t}(\tau)\left\{\hat{X}_\nu,\hat{X}_{\nu'}^{\tau-t}\right\}\right)d\tau - \frac{1}{2M_\nu\omega_\nu}\int_0^t \left\{\hat{F}_\nu^{\tau-t},\hat{\rho}_e^{\tau-t}(\tau)\right\}\sin\omega_\nu(\tau-t)d\tau. \tag{A10}$$

Next, we take the oscillator trace, making the remaining approximations, namely retaining only terms diagonal in ν and ignoring the double (de)excitations $\mathrm{Tr_o}(\hat{a}_\nu\hat{a}_\nu\hat{\rho}_o^{\tau-t}(\tau))$, $\mathrm{Tr_o}(\hat{a}_\nu^\dagger\hat{a}_\nu^\dagger\hat{\rho}_o^{\tau-t}(\tau))$. This gives

$$\mathrm{Tr_o}\sum_{\nu'=1}^{N_o}\left(\left\{\hat{X}_\nu,\hat{X}_{\nu'}^{\tau-t}\right\}\hat{\rho}_o^{\tau-t}(\tau)\right) \approx \frac{\hbar}{M_\nu\omega_\nu}[2N_\nu(\tau)+1]\cos\omega_\nu(\tau-t). \tag{A11}$$

Then Eq. (A10) becomes

$$\hat{\mu}_\nu(t) = \frac{i}{M_\nu\omega_\nu}\int_0^t \left(N_\nu(\tau)+\frac{1}{2}\right)\left[\hat{F}_\nu^{\tau-t},\hat{\rho}_e^{\tau-t}(\tau)\right]\cos\omega_\nu(\tau-t)d\tau - \frac{1}{2M_\nu\omega_\nu}\int_0^t \left\{\hat{F}_\nu^{\tau-t},\hat{\rho}_e^{\tau-t}(\tau)\right\}\sin\omega_\nu(\tau-t)d\tau. \tag{A12}$$

This is Eq. (4).

APPENDIX B: TOTAL-ENERGY CONSERVATION

The time derivative of the total energy of the system is

$$\dot{E} = \mathrm{Tr}_\mathrm{e}(\hat{H}_\mathrm{e}\dot{\hat{\rho}}_\mathrm{e}(t)) + \sum_\nu (\hbar\omega_\nu \dot{N}_\nu(t) - \mathrm{Tr}_\mathrm{e}(\hat{F}_\nu \dot{\hat{\mu}}_\nu(t))). \quad \text{(B1)}$$

Plugging Eq. (2) into the first term of Eq. (B1), and using Eq. (11), we get

$$-\frac{1}{M_\nu \hbar\omega_\nu}\mathrm{Tr}_\mathrm{e}\Big(\big[\hat{F}_\nu, \hat{C}^\nu_\mathrm{c}\big]\hat{H}_\mathrm{e} + i\big[\hat{F}_\nu, \hat{A}^\nu_\mathrm{s}\big]\hat{H}_\mathrm{e}\Big), \quad \text{(B2)}$$

and, with Eq. (12), the second term becomes

$$\frac{1}{M_\nu}\mathrm{Tr}_\mathrm{e}\big(i\hat{F}_\nu \hat{C}^\nu_\mathrm{s} + \hat{F}_\nu \hat{A}^\nu_\mathrm{c}\big). \quad \text{(B3)}$$

Using the time derivative of Eq. (11) together with Eqs. (7) and (10), the third term is

$$-\frac{1}{M_\nu \hbar\omega_\nu}\mathrm{Tr}_\mathrm{e}\Big(\hat{F}_\nu\big(\hat{H}_\Gamma \hat{C}^\nu_\mathrm{c} - \hat{C}^\nu_\mathrm{c}\hat{H}^\dagger_\Gamma\big) + i\hat{F}_\nu\big(\hat{H}_\Gamma \hat{A}^\nu_\mathrm{s} - \hat{A}^\nu_\mathrm{s}\hat{H}^\dagger_\Gamma\big)\Big)$$

$$-\frac{1}{M_\nu}\mathrm{Tr}_\mathrm{e}\big(i\hat{F}_\nu \hat{C}^\nu_\mathrm{s} + \hat{F}_\nu \hat{A}^\nu_\mathrm{c}\big). \quad \text{(B4)}$$

So long as $\hat{I}_\mathrm{leads}\hat{F}_\nu = 0$, we can replace $\hat{H}_\Gamma$ in Eq. (B4) with $\hat{H}_\mathrm{e}$. Then, summing (B2)–(B4) gives $\dot{E} = 0$.

[1] A. P. Horsfield, D. R. Bowler, H. Ness, C. G. Sánchez, T. N. Todorov, and A. J. Fisher, Rep. Prog. Phys. **69**, 1195 (2006).
[2] M. Galperin, M. A. Ratner, and A. Nitzan, J. Phys.: Condens. Matter **19**, 103201 (2007).
[3] W. S. Fann, R. Storz, H. W. K. Tom, and J. Bokor, Phys. Rev. Lett. **68**, 2834 (1992).
[4] W. S. Fann, R. Storz, H. W. K. Tom, and J. Bokor, Phys. Rev. B **46**, 13592 (1992).
[5] T. Ogitsu, Y. Ping, A. Correa, B. I. Cho, P. Heimann, E. Schwegler, J. Cao, and G. W. Collins, High Energy Density Phys. **8**, 303 (2012).
[6] D. Duffy, S. Khakshouri, and A. Rutherford, Nucl. Instrum. Methods Phys. Res., Sect. B **267**, 3050 (2009).
[7] R. Härtle and M. Thoss, Phys. Rev. B **83**, 125419 (2011).
[8] J. T. Lü, M. Brandbyge, P. Hedegard, T. N. Todorov, and D. Dundas, Phys. Rev. B **85**, 245444 (2012).
[9] I. Avigo, R. Cortés, L. Rettig, S. Thirupathaiah, H. S. Jeevan, P. Gegenwart, T. Wolf, M. Ligges, M. Wolf, J. Fink, and U. Bovensiepen, J. Phys.: Condens. Matter **25**, 094003 (2013).
[10] N. H. C. Lewis, H. Dong, T. A. A. Oliver, and G. R. Fleming, J. Chem. Phys. **142**, 174202 (2015).
[11] J. Kogoj, L. Vidmar, M. Mierzejewski, S. A. Trugman, and J. Bonča, arXiv:1509.08431.
[12] N. W. Ashcroft and D. N. Mermin, *Solid State Physics* (Saunders College, Philadelphia, 1976).
[13] T. Frederiksen, M. Paulsson, M. Brandbyge, and A.-P. Jauho, Phys. Rev. B **75**, 205413 (2007).
[14] D. Frenkel and B. Smit, *Understanding Molecular Simulation* (Academic, San Diego, 2002).
[15] S. I. Anisimov, B. L. Kapeliovich, and T. L. Perelman, J. Expt. Theor. Phys. **39**, 375 (1975).
[16] C. P. Flynn and R. S. Averback, Phys. Rev. B **38**, 7118 (1988).
[17] A. Caro and M. Victoria, Phys. Rev. A **40**, 2287 (1989).
[18] M. W. Finnis, P. Agnew, and A. J. E. Foreman, Phys. Rev. B **44**, 567 (1991).
[19] S. Prönnecke, A. Caro, M. Victoria, T. D. de la Rubia, and M. Guinan, J. Mater. Res. **6**, 483 (1991).
[20] D. M. Duffy and A. M. Rutherford, J. Phys.: Condens. Matter **19**, 016207 (2007).
[21] C. P. Race, D. R. Mason, M. W. Finnis, W. M. C. Foulkes, A. P. Horsfield, and A. P. Sutton, Rep. Prog. Phys. **73**, 116501 (2010).
[22] D. Mason, J. Phys.: Condens. Matter **27**, 145401 (2015).
[23] B. I. Cho, K. Engelhorn, A. A. Correa, T. Ogitsu, C. P. Weber, H. J. Lee, J. Feng, P. A. Ni, Y. Ping, A. J. Nelson, D. Prendergast, R. W. Lee, R. W. Falcone, and P. A. Heimann, Phys. Rev. Lett. **106**, 167601 (2011).
[24] E. T. Karim, M. Shugaev, C. Wu, Z. Lin, R. F. Hainsey, and L. V. Zhigilei, J. Appl. Phys. **115** 183501 (2014).
[25] E. Zarkadoula, S. L. Daraszewicz, D. M. Duffy, M. A. Seaton, I. T. Todorov, K. Nordlund, M. T. Dove, and K. Trachenko, J. Phys.: Condens. Matter **26**, 085401 (2014).
[26] A. P. Horsfield, D. R. Bowler, A. J. Fisher, T. N. Todorov, and C. G. Sánchez, J. Phys.: Condens. Matter **16**, 8251 (2004).
[27] A. P. Horsfield, D. R. Bowler, A. J. Fisher, T. N. Todorov, and C. G. Sánchez, J. Phys.: Condens. Matter **17**, 4793 (2005).
[28] L. Stella, M. Meister, A. J. Fisher, and A. P. Horsfield, J. Chem. Phys. **127**, 214104 (2007).
[29] L. Wang, R. Long, and O. V. Prezhdo, Annu. Rev. Phys. Chem. **66**, 549 (2015).
[30] D. G. Cahill, P. V. Braun, G. Chen, D. R. Clarke, S. Fan, K. E. Goodson, P. Keblinski, W. P. King, G. D. Mahan, A. Majumdar, H. J. Maris, S. R. Phillpot, E. Pop, and L. Shi, Appl. Phys. Rev. **1**, 011305 (2014).
[31] D. Mozyrsky and I. Martin, Phys. Rev. Lett. **89**, 018301 (2002).
[32] T. N. Todorov, D. Dundas, J.-T. Lü, M. Brandbyge, and P. Hedegard, Eur. J. Phys. **35**, 065004 (2014).
[33] K. Burke, R. Car, and R. Gebauer, Phys. Rev. Lett. **94**, 146803 (2005).
[34] J. T. Lü, P. Hedegard, and M. Brandbyge, Phys. Rev. Lett. **107**, 046801 (2011).
[35] J. Theilhaber, Phys. Rev. B **46**, 12990 (1992).